Low-cost vision machine for high-throughput automated monitoring of heterotrophic seedling growth on wet paper support

Pejman RASTI[1]

http://perso-laris.univ-angers.fr/~rasti/

Didier DEMILLY[2]

didier.demilly@geves.fr

Landry BENOIT[2]

landry.benoit@univ-angers.fr

Etienne BELIN[1]

etienne.belin@univ-angers.fr

Sylvie DUCOURNAU[2]

sylvie.ducournau@geves.fr

Francois CHAPEAU-BLONDEAU[1]

chapeau@univ-angers.fr

David ROUSSEAU[1]

david.rousseau@univ-angers.fr

[1] LARIS,UMR INRA IRHS, Université d'Angers, 62 avenue Notre Dame du Lac, 49000 Angers, France.

[2] GEVES, Station Nationale d'Essais de Semences (SNES), rue George Morel BP 90024, 49071 Beaucouzé, France.

Abstract

In this communication, we propose a fully automated vision system to monitor the germination and elongation of seedlings positioned in a petri dish. While most existing systems use agar gel as transparent nutritive medium imaged in backlight, we demonstrate that although it provides a reduced contrast, not fully opaque paper can serve as efficient lower-cost medium preventing the well-known problem of seedling joining during elongation. Automatic tracking of elongating seedlings is realized with a minimal path algorithm. The three organs (radicle, hypocotyl, and cotyledon) are then segmented. Validation of the accuracy of the system is provided on sugar beet seedling by comparison with the expert-based ground truth.

1 Plant phenotyping problem and related work

Seedling heterotrophic growth is a crucial stage of the development of plants [19] occuring before the activation of the photosynthetis process (autotrophic growth). After sowing, two successive stages have to occur starting with germination until the radicle protrudes out of the seed coat and then the heterotrophic growth in the soil until the seedling emerges out of the soil. In field conditions, germination and heterotrophic seedling growth stages are not

easily observable since they occur in the soil. As a consequence, diagnosis on sources of seedling emergence failure is difficult, especially the separation of the respective impacts of the two stages in sowing failures. Non-invasive monitoring of seedling growth is accessible in laboratory conditions with computer vision machines. A common imaging system, reported in [1, 2, 5, 6, 7, 10, 11, 12, 18, 21] with various levels of automation, consists in monitoring a set of seedlings positioned on a row in a vertically settled box with agar gel. A backlight system associated with a camera then produces sequences of images of seedling during growth. From such image sequences, the temporal evolution of the length of the seedling is measurable with classical image processing such as binary image skeletonisation.

A limiting factor when considering the whole process of plant preparation and imaging is the use of agar gel as nutritive medium for the seedlings. Agar gel is convenient for imaging seedlings in backlight because it is a transparent medium. However some defaults (air bubbles, scratches, development of pathogens,...) can occur during the preparation of the gel as reported in [4, 18]. These defaults can perturb the quality of the image processing. Even more important, the preparation of the agar gel medium takes time (several hours) and actually represents a, if not the, bottleneck in the monitoring of seedling growth. Last but not least, agar gel leaves the seedling free to move on its surface and it happens from our empirical expertise that very often the seedlings emerging from neighboring seeds tend to join. While some image processing based separation has been developed for crossing seedlings [3], the separation of joining seedlings seems like a very ill-defined problem.

In this work, we propose to use another nutritive medium, cheaper, faster to prepare and that happened to reduce this seedling joining problem. We use a simple non opaque paper as introduced in [14] for single root systems. Because the paper somehow fixes the seedling on the petri dish, the seedling joining is avoided in the presence of multiple seedlings also for the same mechanical reasons movement of hypocotyl and cotyledon are prevented when compared to the freedom to move that seedling have in agar gel. Paper has been used as background earlier [8, 9] in front light and top view with seedlings put at horizontal. In our case the seedling are vertical and the paper is sticking the seedlings to the petri dish. In such conditions, back light provides better contrast than front light. However, although not opaque, the paper reduces the contrast in the acquired images by comparison with the usual agar gel. However, although not opaque, the paper reduces the contrast in the acquired images. The Fisher ratio between background and seedling is found 80.51 for paper while it is found at 558.90 for agar gel. Also, due to mechanical deformation associated with the drying process of the paper and the growth of the seedling, some stripes similar to seedling in terms of size and contrast appear in the image. Figure 1 shows a schematic view of the classical method using agar gel and the faster method using simple wet paper. After some preliminary test (not presented in this short communication) of the available methods of the literature, we identified the need to adapt the image processing tools. Indeed most of the current work monitors root systems during the autotrophic growth [1, 2, 6, 7, 10, 11, 12, 18, 21] while as stressed in [5] there is also biological interest in monitoring the heterotrophic growth. To deal with the specific anatomical organs visible during heterotrophic growth and the low-contrasted and cluttered images, we propose a computer vision algorithm presented in the following section which aims at tracking and segmenting each organ (radicle, hypocotyl and cotyledon) of a seedling as shown in Fig. 2.
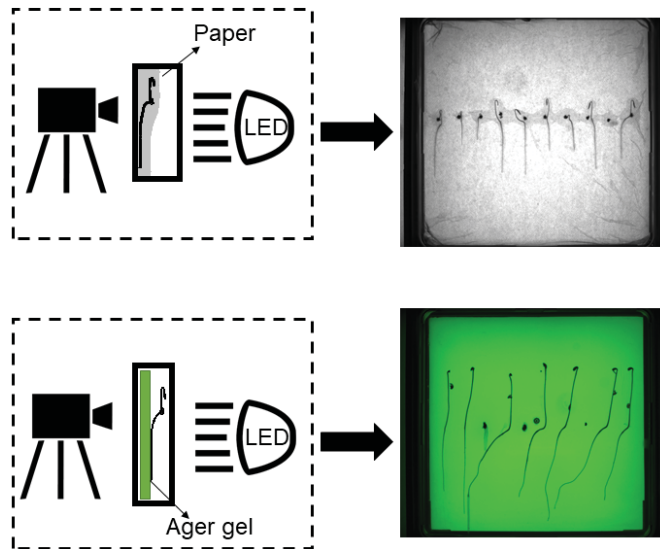
Figure 1: The imaging system with simple paper used in this report compared with the usual longer to prepare agar gel as support. The LED light is a back light considered for a petri dish, and camera is capturing images from front side of a petri dish.
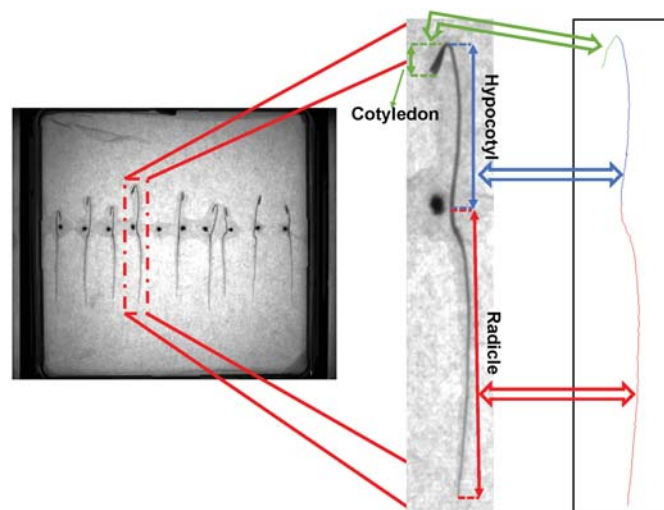
Figure 2: Overview of the segmentation of the three seedling organs.

2 Computer vision approach

Dry seedlings are positioned on a wet paper inside a petri dish imaged with a 2050 pixels by 2448 pixels camera. The lighting is backlight with an inactinic LED [5]. Images are acquired at a frame rate of 1 image every 240 minutes (min) during 464 hours over 18 days. For illustration, as shown in Fig.3 with sugar beet seeds, this produces sequences of images with rather low contrast specially at the root tip.

2.1 Image processing

As shown in Fig. 4 the automatic vision system for tracking growth of seedlings and detecting each organ consists in several steps starting at seed detection up to organs length measurements. Each step is described separately in the following sub-sections.
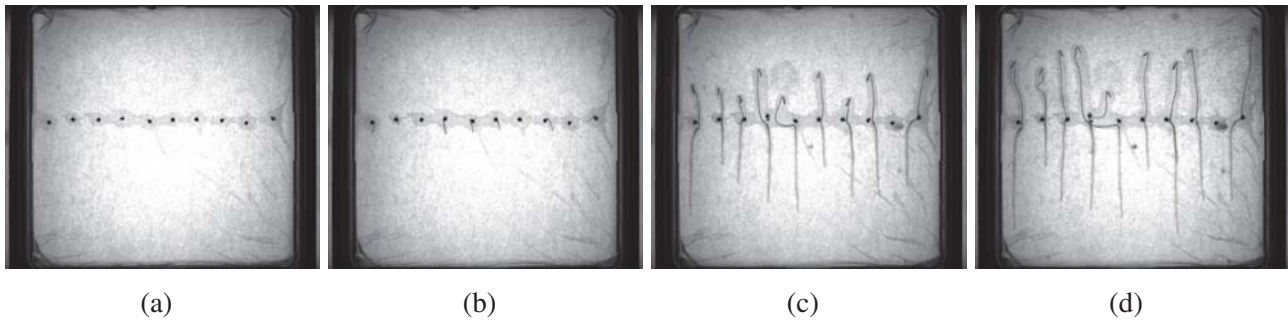
Figure 3: Four gray level images of seedlings of suger beet during the elongation phase, from (a) to (d), acquired at the time of $t = 0$ min , $t = 5040$ min, $t = 17040$ min, $t = 28080$ min using our imaging system.
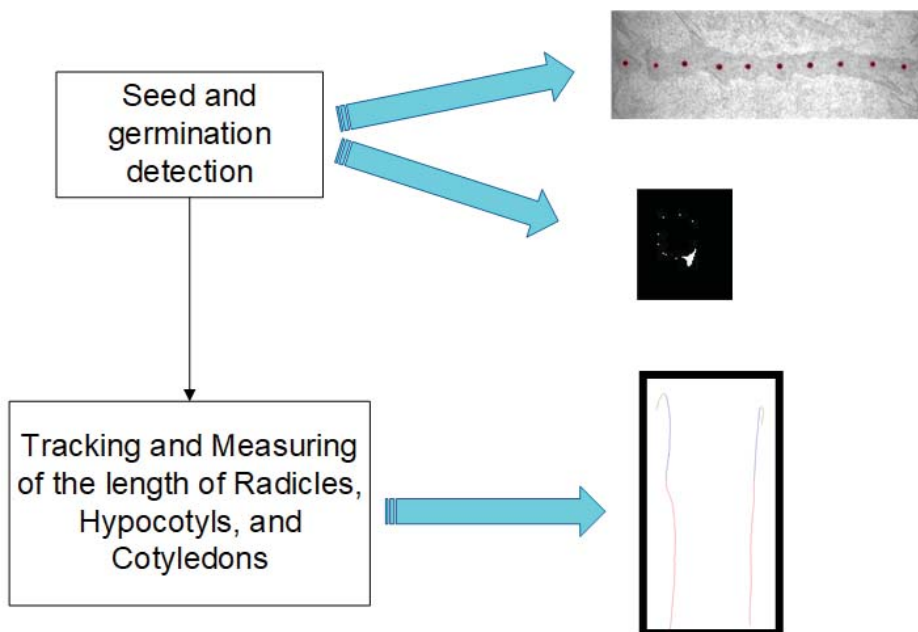
Figure 4: Block diagram of the automatic vision system.

2.1.1   Seed and germination detection

Figure 5 shows our pipeline of seed and germination detection process. In the beginning, a pre-processing step is considered on all images in a sequence. In this step, frame borders are cropped and seeds and seedlings with a background are kept for further analyses. A simple Otsu threshold [15] is applied to the first image ($t = 0$ min) in order to segment seeds (before germination) from background. The Otsu thresholding can be efficient as the contrast of seeds is good enough for a segmentation. Then the initial center coordinates of each seed are recorded to use for germination detection step. Figure 6 shows a sample of seeds detection at the first image ($t = 0$ min) of each sequence.

At the second step, we find the time of germination (the area where the radicle and hypocotyl pop out of the seed) of each seed. The germination time in a sequence can be detected by measuring the movement of the initial center of the seed in a way that the Euclidean distance d_g of the movement of the center of the seed at the time of $t = 0$ min and
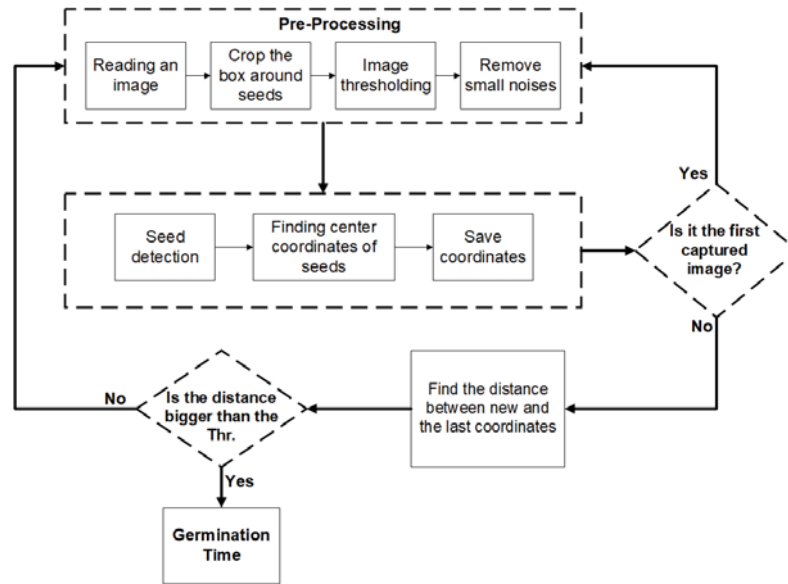
Figure 5: Flowchart of germination detection approach.
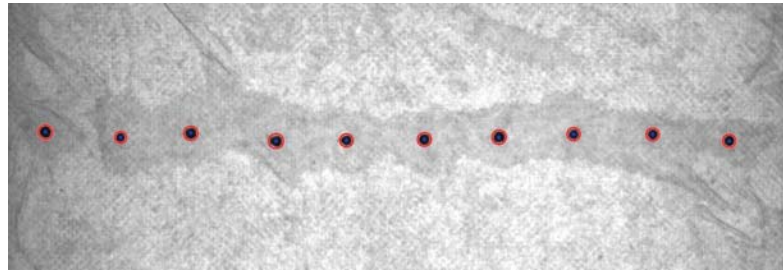
Figure 6: Output image after the first step.

$t = n$ min is measured by equation

$$d_g = \sqrt{\left(x_{s_{t=0}} - x_{s_{t=n}}\right)^2 + \left(y_{s_{t=0}} - y_{s_{t=n}}\right)^2} \tag{1}$$

where distance d_g is a simple Euclidean distance, $(x_{s_{t=0}}, y_{s_{t=0}})$ are the initial center's coordinates of each seed and $(x_{s_{t=n}}, y_{s_{t=n}})$ of are the center's coordinates at the time of n of the correspondent seed. A seed is germinated if the distance passes a specific threshold. With the time step of 240 minutes used in our experiment, a threshold of $thr = 2$ pixels is empirically chosen for an efficient detection of germination.

The next step after germination detection is to specify the location of the germination area $G = \{g_{1_{x,y}}, g_{2_{x,y}}, ..., g_{n_{x,y}}\}$ where $g_{i_{x,y}}$ are pixels belonging to the germination area. This is achievable by simply subtracting the image at the time of germination $t = n$ from the last image before germination $t = n - 240$. This subtraction removes all seed areas except germination area plus small points (noises) at the borders of the seed. These small noises can easily be removed by keeping the biggest connected component as the germination area $G = \max(C_i)$ where C_i represent the size (number of pixels) of connected components. Figure 7 shows three examples of this step for detecting germination area.

As shown in [5], a gravitropism prior enables to use this germination area to fix the separation between the radicle which grows down and the hypocotyl which grows up. In order to specify a specific point (pixel) as the separation point between radicle and hypocotyl , the central pixel of G is selected and recorded as the germination point $g_{s_{x,y}}$.
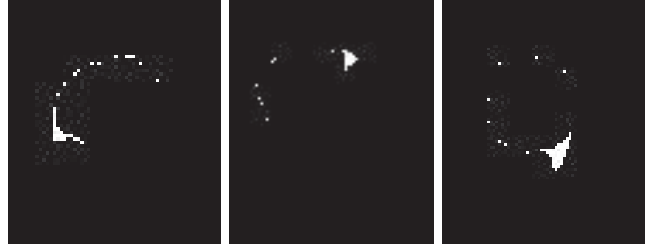
Figure 7: Examples of the detection of germination coordinates.

2.1.2 Seedling tracking

As a pre-step here, a specific patch is considered around each seed/seedling based on its location in each frame of the sequence and all pixels out of this patch are removed to make sure that additional noises can not disturb the tracking of seedlings. In order to track the growth of seedlings, a minimal path algorithm [20] is adopted and applied on each seedling separately. Considering a starting point and ending point in a shape H, the minimal path is a geodesic [13] between these two points. Its extraction can be seen as a front propagation problem [16] from one point to the other. The distance transform maps each image pixel into its smallest distance to regions of interest [17]. Tracing the distance map from a specified point to a referred one will give a geodesic between these two points. To force the geodesic to be near the centerline of each organ, a weighted distance map WDT related to the grey level of each organ is computed. Let H be the studied greyscale organ, $H(a)$ the normalized intensity at pixel $a \in H$. The WDT of H is given by:

$$WDT(a) = DT(a) \times e^{-\eta \times H(a)^2} \tag{2}$$

with $DT(a) = \min_{p \in S}((d(p,a)))$ where $d()$ is the Euclidian distance and η represents a weighting coefficient which is empirically chosen for each image.

The set of maximal geodesics is extracted as follow: we propagate a front within each organ from germination point $g_{s_{(x,y)}}$, and locate the maxima $Ei = max(WDT(g_{s_{(x,y)}}))$. A geodesic $Path_i$ is built considering $g_{s_{(x,y)}}$ (as a starting point for both radicle and hypocotyl) and ending point $E_i = \{E_1, E_2\}$ where E_1 is the ending points of radicle and E_2 represents the ending points of hypocotyl. In order to detect these ending points, the Otsu threshold technique is applied in each seedlings to segment the whole shape of them, then pixels with the lowest and the highest positions in a vertical direction are considered as E_1 and E_2 respectively. Then $Path_i$ subtracted from the shape $R = HDil_B(Path_i)$ where $Dil_B(Path_i)$ is the morphological dilation operation and B a disk of radius b corresponding to the observed shape width. If R is empty, the process is stopped. This means that the set of the extracted maximal geodesics (here $Path_i$) covers the entire organs. If R is not empty (which means the cotyledon is appeared), maximal geodesics are iteratively extracted from the remaining organ. $Path_{i+1}$ is then computed from the remaining shape R.

It should be mentioned that the seed corresponding to each seedling is removed (called as the seed removing process) before calculating of $Path_i$ as the contrast of the seed is much higher than its seedling and the minimal path always passes through the seed.

2.1.3 Organ segmentation

At the end of the tracking process, three paths are extracted as $Path_i = \{Path_1, Path_2, Path_3\}$. These paths enable us to segment the different organs of a seedlings based on biological knowledge as radicle and hypocotyl are connected on the germination point. The hypocotyl organ is segmented by the path between $g_{s_{(x,y)}}$ and E_2 which is shown as $Path_2$. Similarly $Path_1$ which is the path between $g_{s_{(x,y)}}$ and E_1 is used to segment the radicle organ. As the cotyledon is located in the continuity of the hypocotyl at the top part of a seedling, $Path_3$ is considered as the path for the cotyledon of a seedling.

3 Results

At the end of the process of tracking and segmentation, two reports followed by four curves are generated for each series of seedling sequences which can be used for further analysis such as growth rate, germination time, etc. The first report consists of the germination time of each seed and the length of each organ after three, seven, and fourteen days after germination in pixels and millimeter (mm). This report can also point an anomaly during the seedlings growth such as late germination (even no germination), or any crossing between two seedlings or fusion of two or more seedlings. The second report consists of the length of each organ during their growth based on tracking results of each image in a sequence. This report can give the required information to analyze the growth behavior of seedlings at any time of their growth. Based on this report three curves of the growth behavior of each organ over the time plus a curve of the growth behavior of all organs together (total seedling length) are produced as shown in Fig. 8.
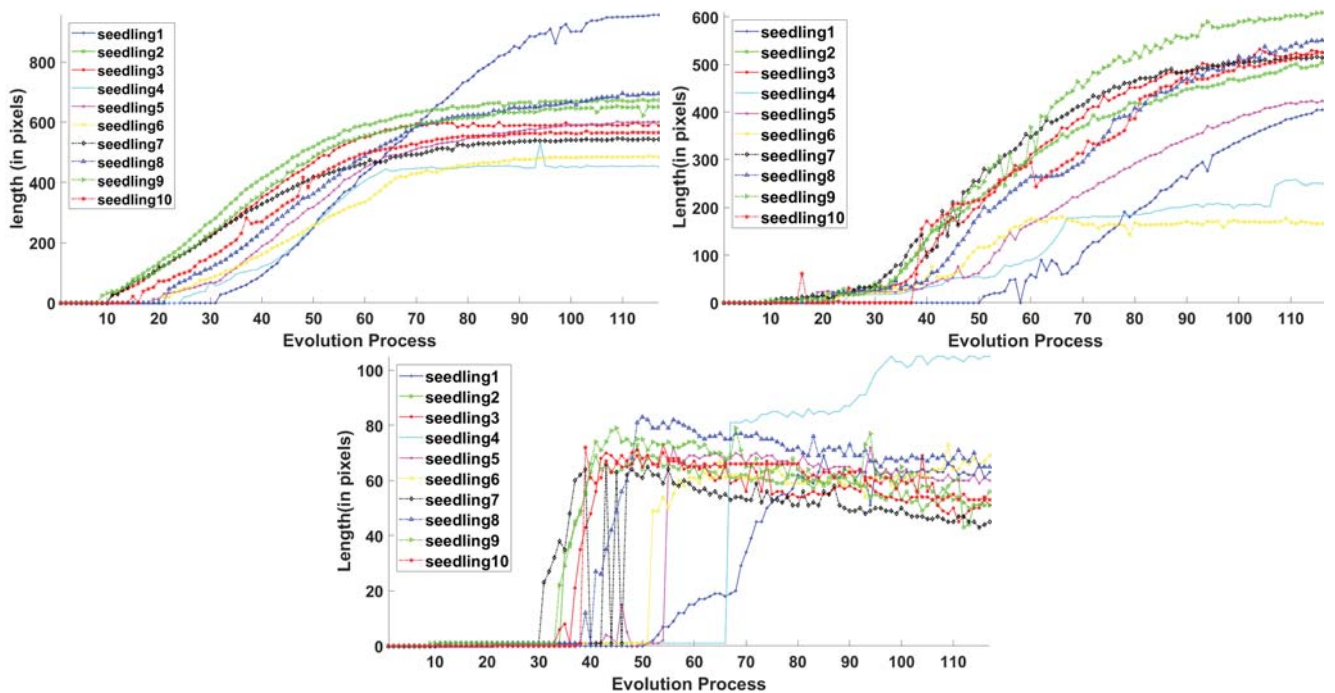
Figure 8: Length (in pixels) of each organ of 10 seedlings in one capturing series over the time ($\times$ 240 min). Top left curves show the length of radicles, top right curves illustrate the length of hypocotyl, and the bottom center one represents the length of cotyledon.

3.1   Validation

In order to validate the algorithm presented in this communication, a comparison with manual measurements of organs has been done. This validation has been done on four series of captured images where each captured series consists of a sequence of 117 images of 10 seeds. In total, the growth length of 40 seedlings is used to estimate the accuracy of the algorithm. The first comparison is done on the germination time. The results show that the automatically estimated germination is well-correlated to the manual detection in Fig. 9 with a small underestimation though since the slope of the curve is slightly below 1.
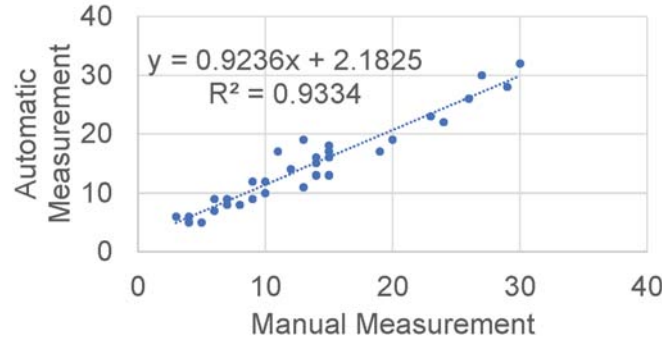
Figure 9: Comparison of germination time (in minutes) between manual detection and the algorithm detection for all seeds.

In order to validate the length measurement accuracy of the algorithm as well, the length of radicle, hypocotyl and cotyledon of all 40 seedlings 14 days after germination have been measured in millimeter by both our algorithm and manually. The experimental results at Fig. 10(a) shows that except one radicle with the maximum difference of $14mm$ between two different measurements, the rest of radicles have a different length of less than $2mm$ on an average. Figures 10(b) and 10(c) show that except for seedling number 20 measurements are very close to the manual measurement.

As a limitation of the algorithm (it is shown in figure 10 as well), rarely there are big differences between manual and automatic measurement such as radicle 28, or hypocotyl 20. Theses differences caused by some limitation on the algorithm. For example, there is a seed movement at the seedling number 20 (which the algorithm is not able to detect it yet), so due to seed removing process, some parts of the seedling will be eliminated at the center of the seedling which makes it difficult for the algorithm to track the growth of the seedling. Figure 11 shows an example of this problem. In this version of the algorithm, these type of seedlings are reported as abnormal seedlings but in the future work, a seed movement detection will be added to the algorithm to avoid these problems.

4   Conclusion

We have demonstrated the possibility to efficiently perform organ segmentation and tracking in sequences of images of seedling elongation while using a simple wet paper support much faster to prepare than the common approach based on agar gel. The approach, which constitutes a possible very valuable improvement and reduction cost, is based on the use of a minimal path tracking algorithm on multiple seedlings put in a petri dish during heterotrophic growth and under inactinic backlight. This can be considered as an extension of

(a)

(b)

(c)
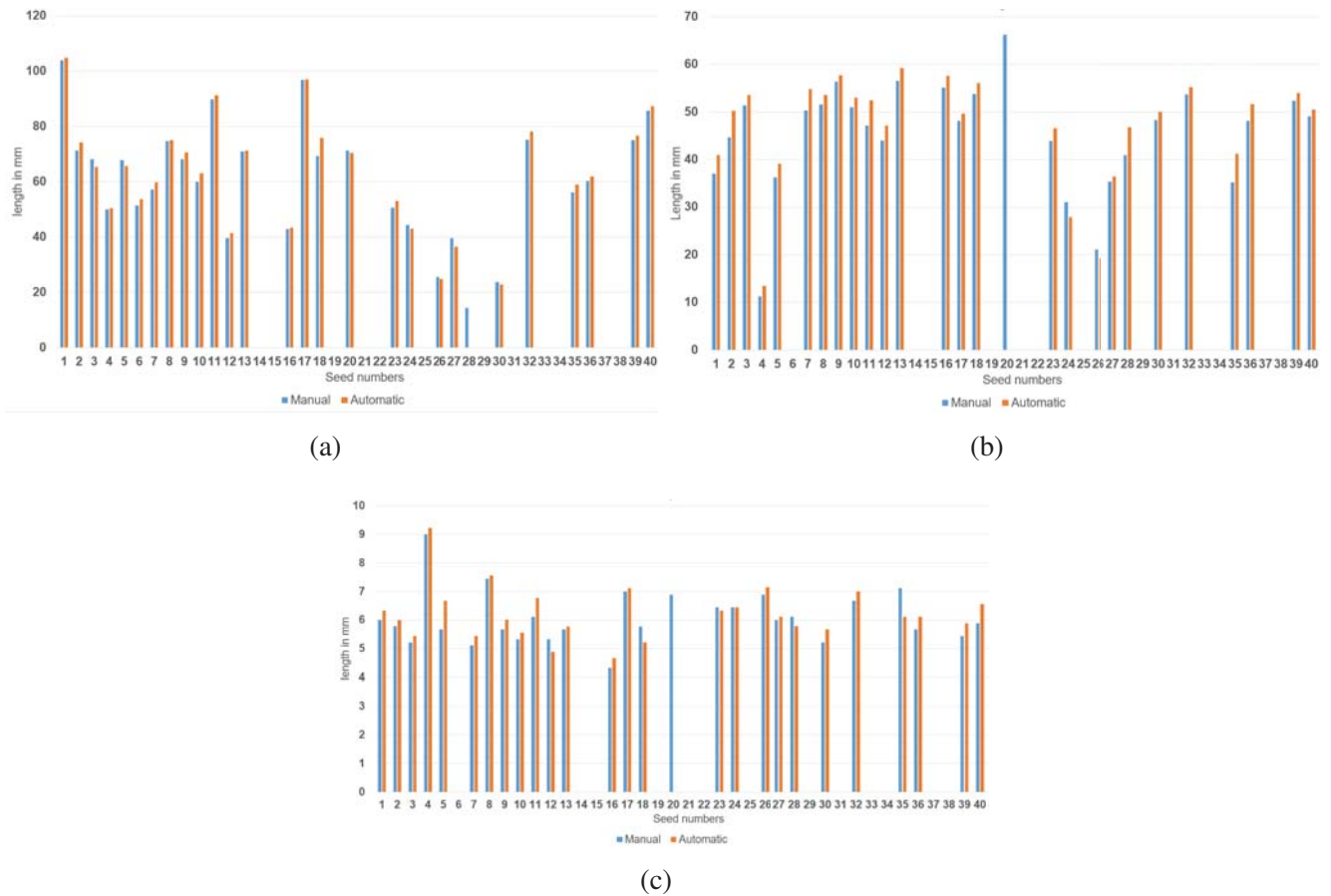
Figure 10: a,b, and c shows a comparison of the length (in mm) of radicle, hypocotyl, and cotyledon respectively between manual detection and automated detection for all seeds.

Figure 11: Elimination of the central part of a seedling during the seed removing process .

recently related propositions to use cheaper nutritive medium than agar gel in plant computer vision including opaque wet blotter [6] in front light or paper [14] during a different stage of development of the seedling (autotrophic growth). Perspectives of this preliminary work include on the experimental part the comparative investigation of the various media (agar gel, wet blotter, wet paper) in terms of germination dynamics with various species. Also, on the computer vision part, we envision to open a challenge on our low contrast images to allow the comparison in terms of measuring accuracy and computation time on alternative solutions.

5   Acknowledgement

References

[1] Renaud Bastien, David Legland, Marjolaine Martin, Lucien Fregosi, Alexis Peaucelle, Stéphane Douady, Bruno Moulia, and Herman Höfte. Kymorod: a method for automated kinematic analysis of rod-shaped plant organs. *The Plant Journal*, 88(3):468–475, 2016.

[2] E Belin, David Rousseau, Julio Rojas-Varela, Didier Demilly, M-H Wagner, M-H Cathala, and Carolyne Dürr. Thermography as non invasive functional imaging for monitoring seedling growth. *Computers and electronics in agriculture*, 79(2):236–240, 2011.

[3] Landry Benoit, David Rousseau, Etienne Belin, Didier Demilly, S Ducournau, François Chapeau-Blondeau, and C Dürr. Locally oriented anisotropic image diffusion: application to phenotyping of seedlings. In *8th international conference on Computer Vision Theory and Applications (VISAPP 2013), Barcelona*, pages 21–24, 2013.

[4] Landry Benoit, David Rousseau, Étienne Belin, Didier Demilly, and François Chapeau-Blondeau. Simulation of image acquisition in machine vision dedicated to seedling elongation to validate image processing root segmentation algorithms. *Computers and electronics in agriculture*, 104:84–92, 2014.

[5] Landry Benoit, Étienne Belin, Carolyne Dürr, François Chapeau-Blondeau, Didier Demilly, Sylvie Ducournau, and David Rousseau. Computer vision under inactinic light for hypocotyl–radicle separation with a generic gravitropism-based criterion. *Computers and Electronics in Agriculture*, 111:12–17, 2015.

[6] Lionel X Dupuy, Gladys Wright, Jacqueline A Thompson, Anna Taylor, Sebastien Dekeyser, Christopher P White, William TB Thomas, Mark Nightingale, John P Hammond, Neil S Graham, et al. Accelerating root system phenotyping of seedlings through a computer-assisted processing pipeline. *Plant methods*, 13(1):57, 2017.

[7] Andrew French, Susana Ubeda-Tomás, Tara J Holman, Malcolm J Bennett, and Tony Pridmore. High-throughput quantification of root growth using a novel image-analysis tool. *Plant physiology*, 150(4):1784–1795, 2009.

[8] Tania Gioia, Anna Galinski, Henning Lenz, Carmen Müller, Jonas Lentz, Kathrin Heinz, Christoph Briese, Alexander Putz, Fabio Fiorani, Michelle Watt, et al. Growscreen-page, a non-invasive, high-throughput phenotyping system based on germination paper to quantify crop phenotypic diversity and plasticity of root traits under varying nutrient supply. *Functional Plant Biology*, 44(1):76–93, 2017.

[9] A Hund, S Trachsel, and P Stamp. Growth of axile and lateral roots of maize: I development of a phenotying platform. *Plant and Soil*, 325(1-2):335–349, 2009.

[10] H Ishikawa and ML Evans. Novel software for analysis of root gravitropism: comparative response patterns of arabidopsis wild-type and axr1 seedlings. *Plant, cell & environment*, 20(7):919–928, 1997.

[11] Mordecai J Jaffe, Andrew H Wakefield, Frank Telewski, Edward Gulley, and Ronald Biro. Computer-assisted image analysis of plant growth, thigmomorphogenesis, and gravitropism. *Plant physiology*, 77(3):722–730, 1985.

[12] K Kimura and S Yamasaki. Accurate root length and diameter measurement using nih image: use of pythagorean distance for diameter estimation. *Plant and soil*, 254(2): 305–315, 2003.

[13] Christian Lantuéjoul and Serge Beucher. On the use of the geodesic metric in image analysis. *Journal of Microscopy*, 121(1):39–49, 1981.

[14] Chantal Le Marié, Norbert Kirchgessner, Daniela Marschall, Achim Walter, and Andreas Hund. Rhizoslides: paper-based growth system for non-destructive, high throughput phenotyping of root development by means of image analysis. *Plant Methods*, 10(1):13, 2014.

[15] Nobuyuki Otsu. A threshold selection method from gray-level histograms. *IEEE transactions on systems, man, and cybernetics*, 9(1):62–66, 1979.

[16] Gabriel Peyré and Laurent Cohen. Heuristically driven front propagation for geodesic paths extraction. In *Variational, Geometric, and Level Set Methods in Computer Vision*, pages 173–185. Springer, 2005.

[17] Azriel Rosenfeld and John L Pfaltz. Distance functions on digital pictures. *Pattern recognition*, 1(1):33–61, 1968.

[18] Ram Subramanian, Edgar P Spalding, and Nicola J Ferrier. A high throughput robot system for machine vision based plant phenotype studies. *Machine Vision and Applications*, 24(3):619–636, 2013.

[19] L Taiz and E Zeiger. Plant physiology 5th ed. *Sunderland, MA: Sinauer Associates*, 2010.

[20] Luc Vincent. Minimal path algorithms for the robust detection of linear features in gray images. *Computational Imaging and Vision*, 12:331–338, 1998.

[21] A Walter, H Spies, S Terjung, R Küsters, N Kirchgeßner, and U Schurr. Spatio-temporal dynamics of expansion growth in roots: automatic quantification of diurnal course and temperature response by digital image sequence processing. *Journal of experimental botany*, 53(369):689–698, 2002.